

Supplement of Biogeosciences, 16, 3801–3834, 2019
<https://doi.org/10.5194/bg-16-3801-2019-supplement>
© Author(s) 2019. This work is distributed under
the Creative Commons Attribution 4.0 License.



Supplement of

Variations in dissolved greenhouse gases (CO₂, CH₄, N₂O) in the Congo River network overwhelmingly driven by fluvial-wetland connectivity

Alberto V. Borges et al.

Correspondence to: Alberto V. Borges (alberto.borges@uliege.be)

The copyright of individual parts of the supplement might differ from the CC BY 4.0 License.

Figure S1: Comparison of the partial pressure of CO₂ (pCO₂ in ppm) measured in the home laboratory by gas chromatography (GC) from serum bottles poisoned with HgCl₂ (+HgCl₂ & GC) with the pCO₂ measured directly in the field with an infra-red gas analyzer (IRGA, in most cases a Li-Cor Li-840) (direct & IRGA) as function of total alkalinity (TA in μmol kg⁻¹) and as function of pCO₂ (direct & IRGA) in the Congo River during high water (03/12/2013-19/12/2013) and falling water (10/06/14-30/06/14) periods. The increase of pCO₂ (+HgCl₂ & GC) compared to pCO₂ (direct & IRGA) is attributed to the precipitation of HgCO₃ that leads to a shift of equilibrium of HCO₃⁻ towards CO₂ ($\text{Hg}^{2+} + 2\text{HCO}_3^- = \text{HgCO}_3 + \text{CO}_2 + \text{H}_2\text{O}$). This is consistent with the increase of the difference between pCO₂ (+HgCl₂ & GC) and pCO₂ (direct & IRGA) with TA that mainly corresponds to HCO₃⁻ in freshwater. As the highest pCO₂ values are observed in blackwaters with low to nil TA values, the difference between pCO₂ (+HgCl₂ & GC) (direct & IRGA) is highest at low pCO₂ (direct & IRGA) values.

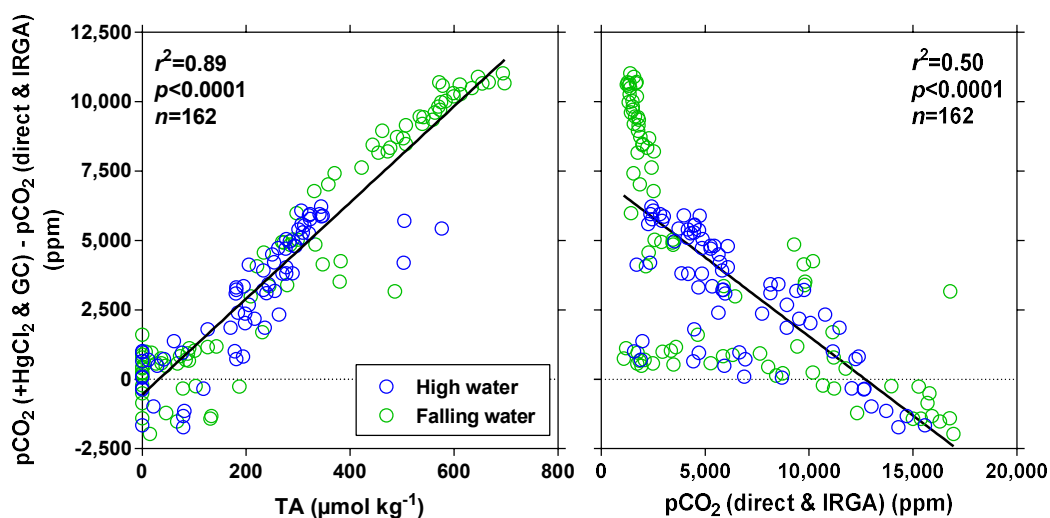


Figure S2: Comparison of measurements of turbidity with the YSI 6600 multiparameter probe (nephelometric turbidity unit (NTU)) and discrete total suspended matter (TSM in mg L^{-1}) in the Congo River during high water (03/12/2013-19/12/2013) and falling water (10/06/14-30/06/14) periods.

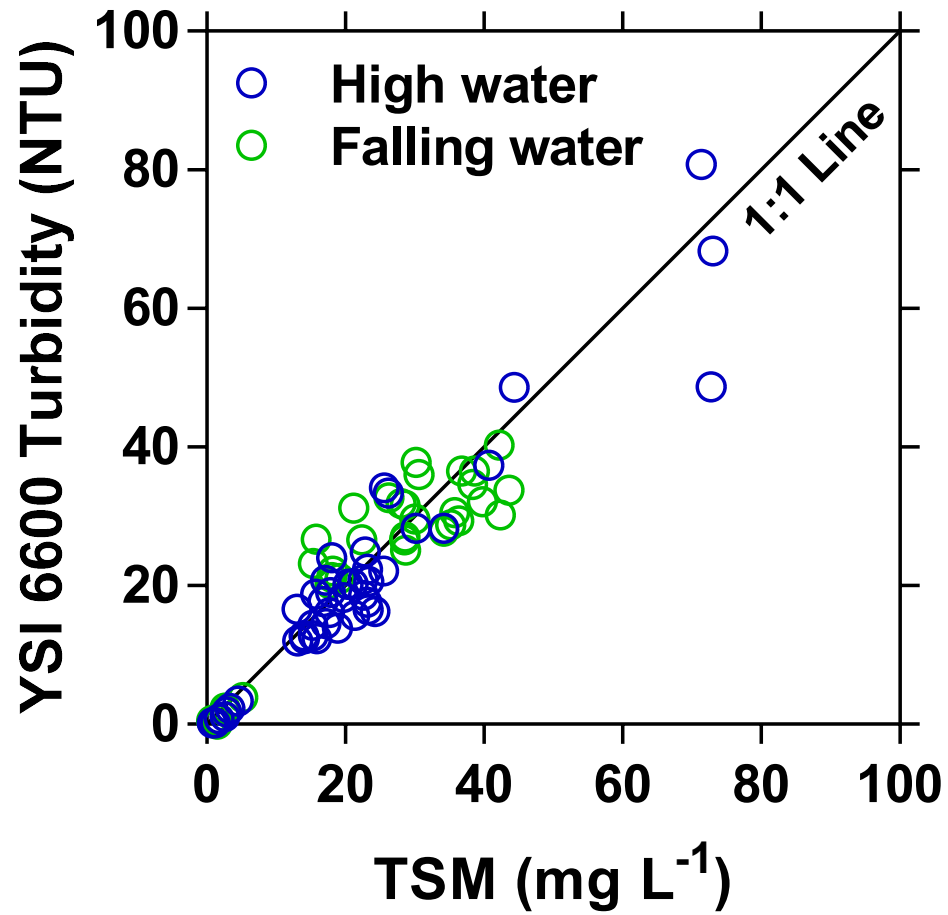


Figure S3: Comparison of measured and modelled primary production ($\text{mmol m}^{-2} \text{d}^{-1}$). Data points corresponding to Chlorophyll-a concentrations $< 0.3 \mu\text{g L}^{-1}$ are shown by red dots. Solid line corresponds to 1:1 line and dotted line corresponds to the linear regression.

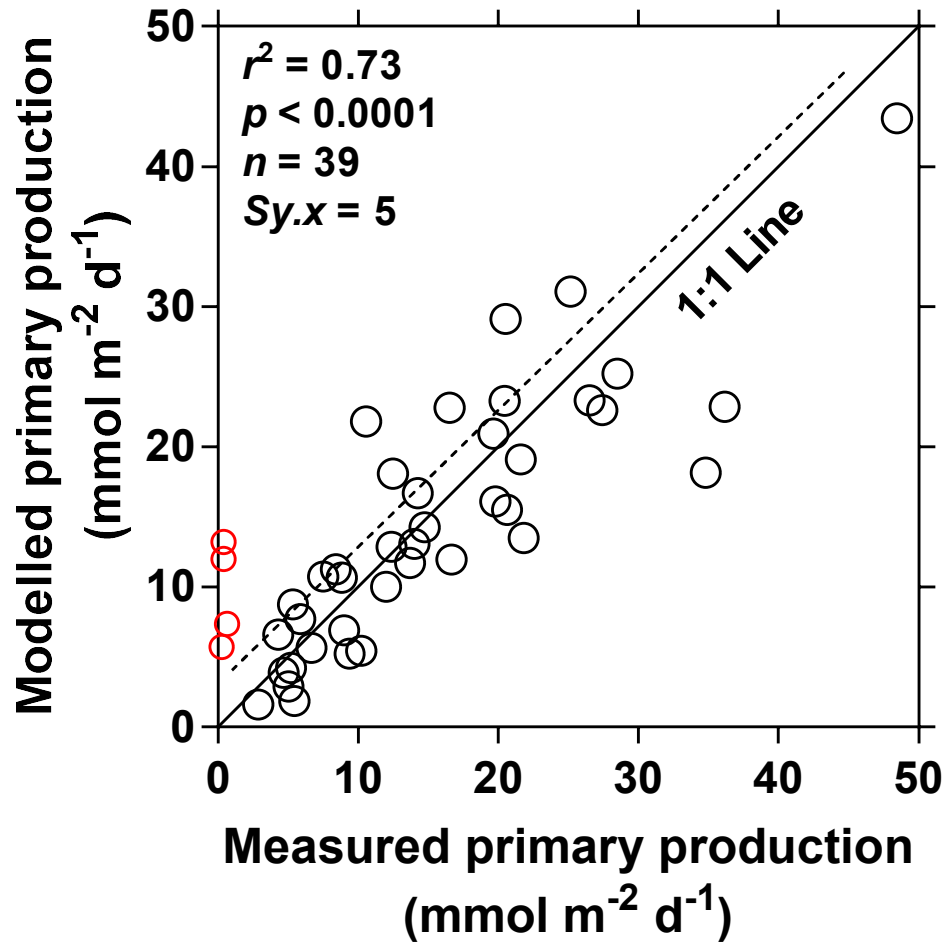


Figure S4: Partial pressure of CO₂ (pCO₂ in ppm) as function of dissolved O₂ saturation level (%O₂ in %), total suspended matter (TSM in mg L⁻¹), pH and specific conductivity in the Congo River during high water (03/12/2013-19/12/2013, *n*=10,505) and falling water (10/06/14-30/06/14, *n*=12,968) periods.

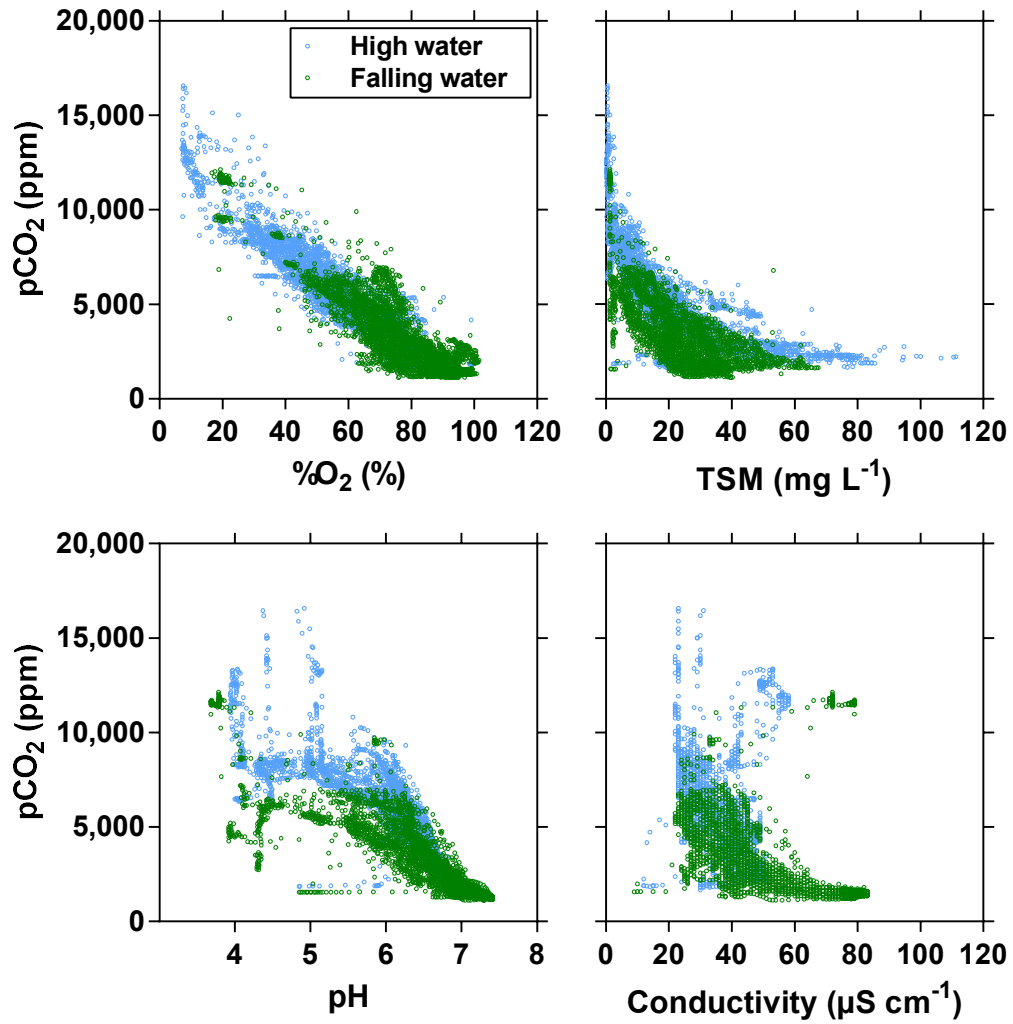


Figure S5: Fraction of oxidized CH₄ computed from the carbon stable isotope composition of CH₄ in surface waters of mainstem of the Congo River (black symbols) and tributaries (green symbols) as a function of dissolved CH₄ concentration (nmol L⁻¹) and as function of the distance upstream of Kinshasa, obtained along a longitudinal transect along the Congo River from Kisangani (10/06/14-30/06/14). Dotted line indicates linear regression.

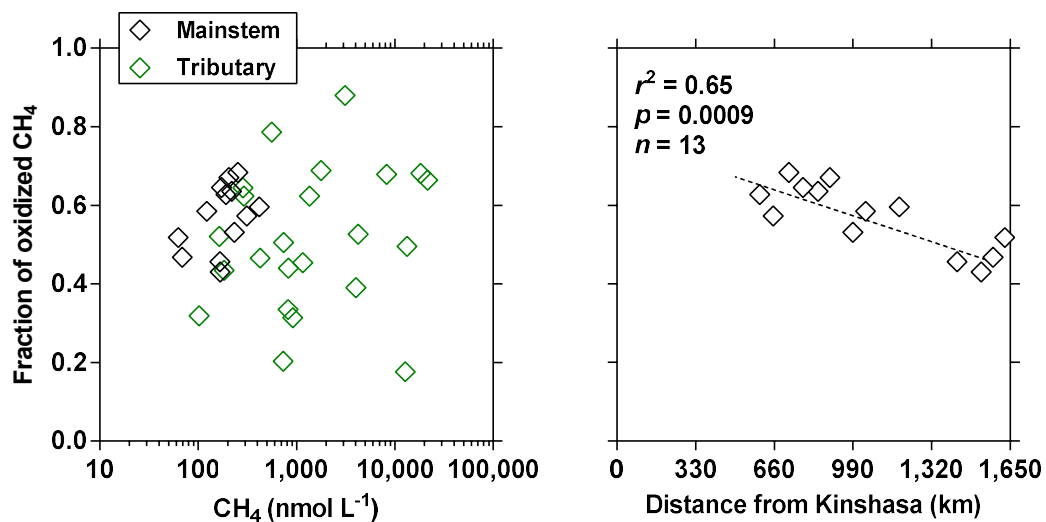


Figure S6: Photographs of several macrophytes present in the Congo River network.
Photo credits AV Borges and F Darchambeau.



- 1 - *Vossia cuspidata***
- 2 - *Eichhornia crassipes***
- 3 - *Salvinia auriculata***
- 4 - *Azolla pinnata***

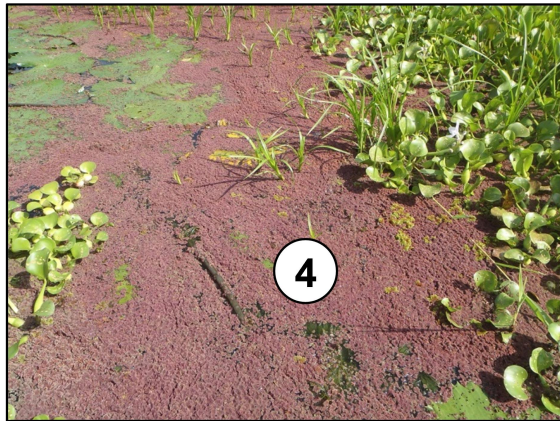


Figure S7: CH₄ oxidation rates (nmol L⁻¹ d⁻¹) as a function of dissolved CH₄ concentration (nmol L⁻¹) in several sites of the Congo River network (16/04/15-06/05/15)

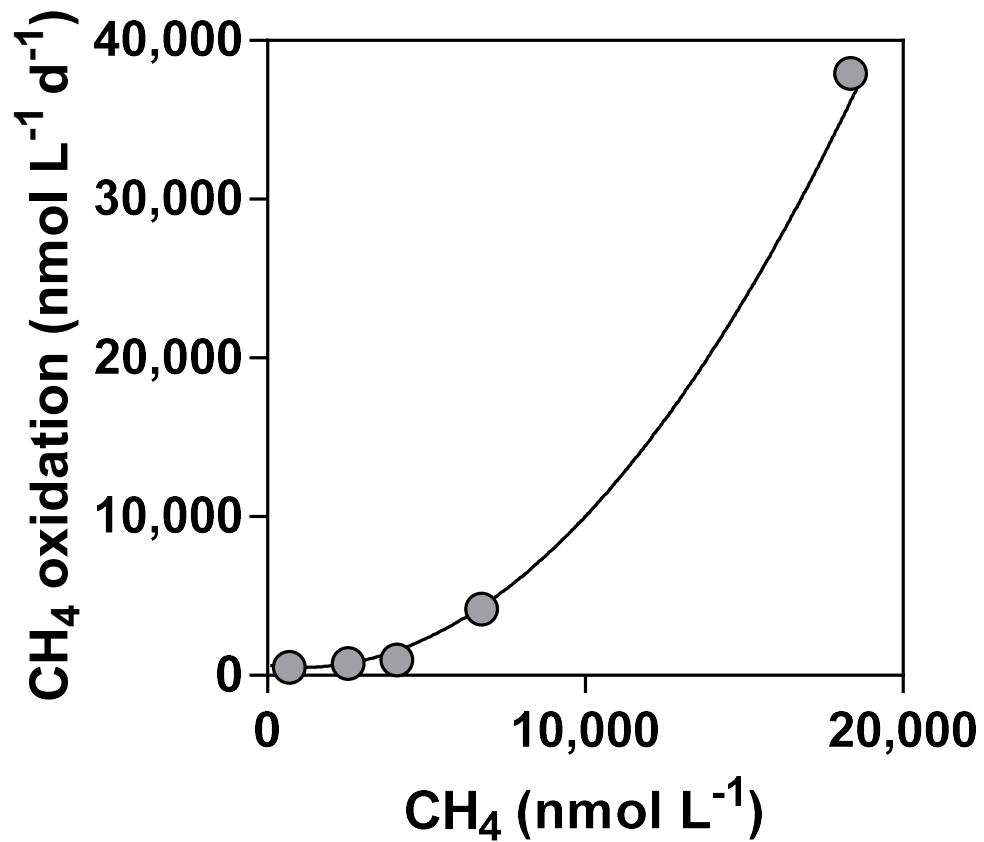


Figure S8: True colour remote sensed images (Google Earth ©) of the confluence of the Congo River mainstem with the Itimbiri and Ruki Rivers and outlet of Lake Tumba.



Figure S9: Photographs of *Vossia cuspidata* meadows at the mouth of the Ruki (top) and in the Congo mainstem (bottom). Photo credits AV Borges



Figure S10: Community respiration ($\text{mmol m}^{-3} \text{d}^{-1}$) as a function of dissolved organic carbon (DOC in mg L^{-1}). Green dots indicate individual measurements, filled dots indicate binned medians by bins of $5 \text{ mmol m}^{-3} \text{d}^{-1}$ of CR. Error bars indicate first and third quartile. DOC values $> 20 \text{ mg L}^{-1}$ are mostly from streams draining the CCC.

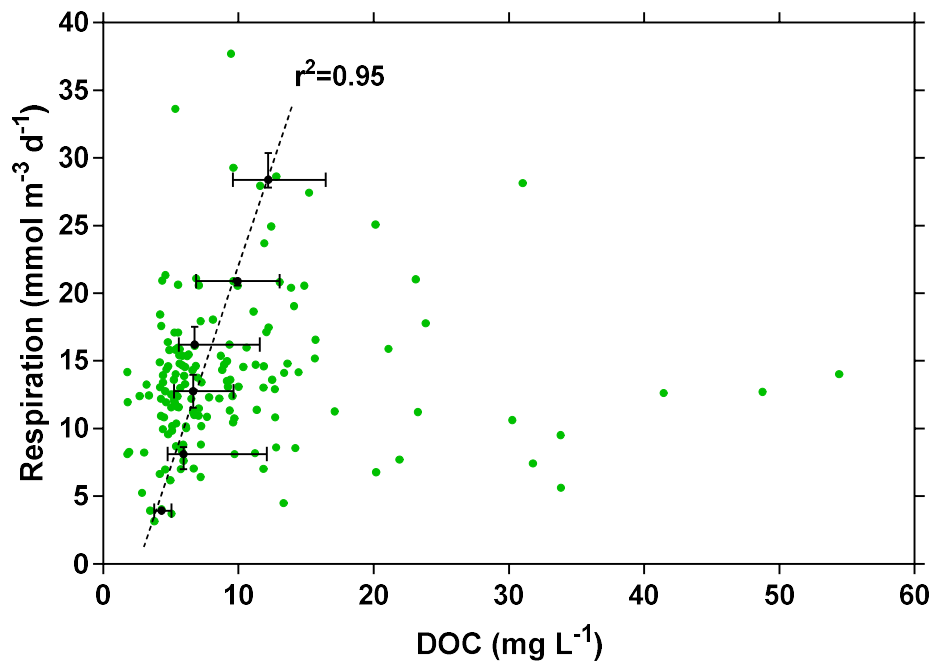


Figure S11: Comparison of the partial pressure of CO₂ (pCO₂ in ppm), dissolved oxygen concentration (O₂ in μmol L⁻¹), water temperature and specific conductivity (μS cm⁻¹) acquired at the anchoring site on shore (typically around 17h00 universal time (UT), just before dusk, “Afternoon”) with the data on the same spot the next day (typically around 04h30 UT, just after dawn, “Morning”). Red dots were excluded from the statistical test.

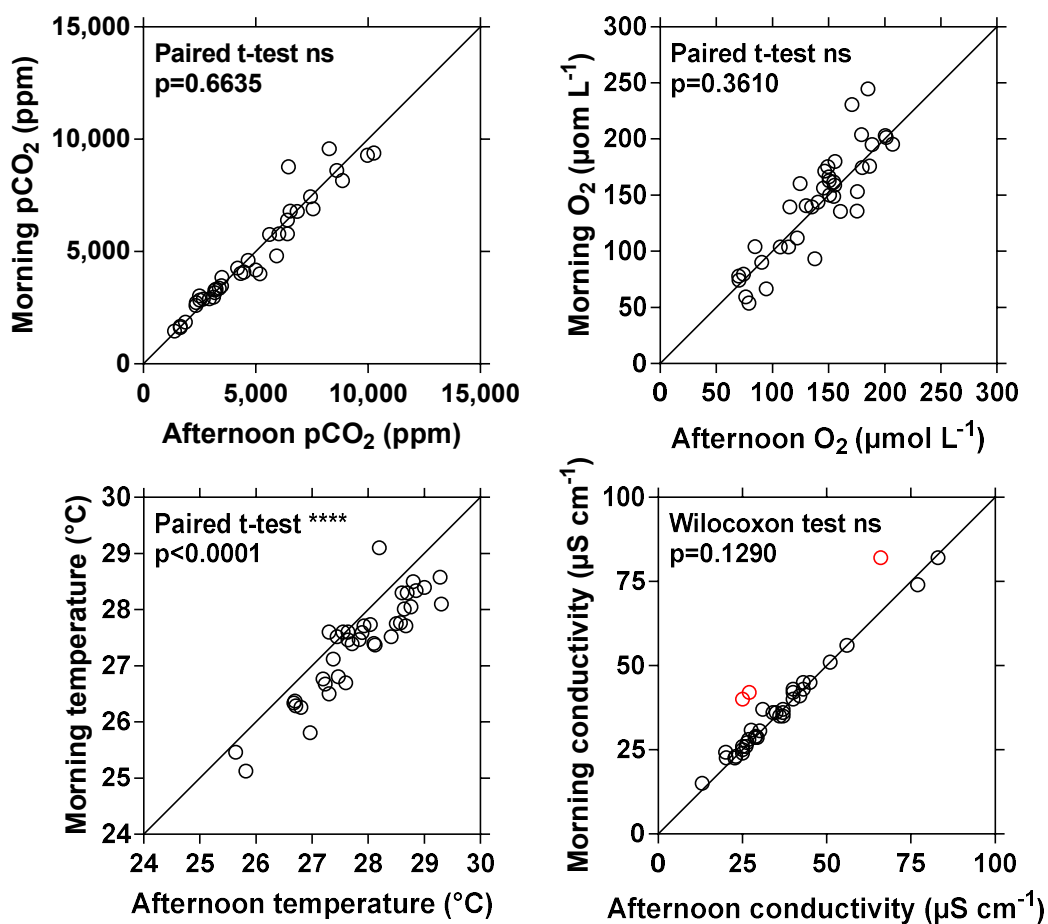


Figure S12: Carbon stable isotope composition of dissolved inorganic carbon (DIC) ($\delta^{13}\text{C-DIC}$ in ‰) for a total alkalinity (TA) to DIC ratio ($\mu\text{mol}:\mu\text{mol}$) equal to zero in surface waters of the Congo River network as a function of the fraction of C_4 vegetation on the catchment based on the geospatial model of Still and Powell (2010) and the fraction of savannah on the catchment extracted from Global Land Cover 2009.

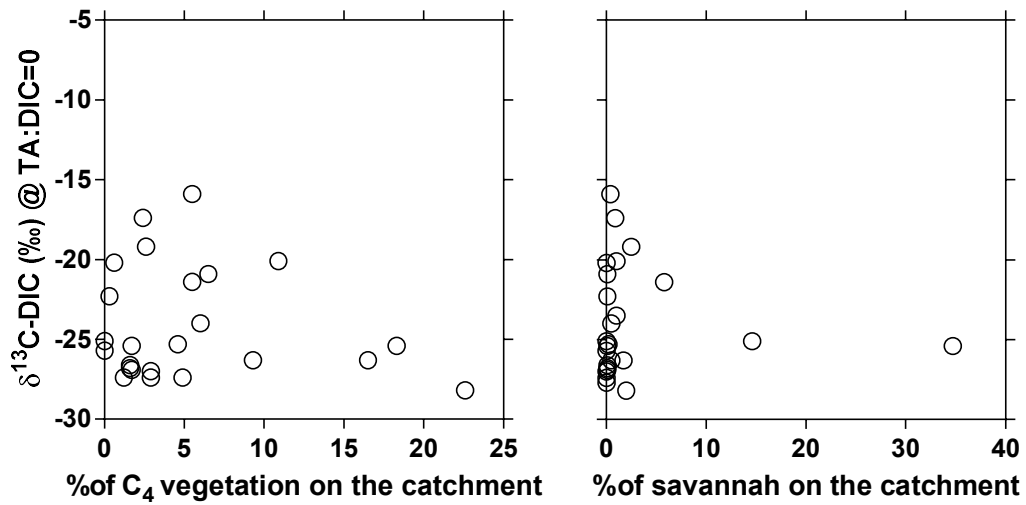


Figure S13: Annual average of dissolved N_2O concentration (N_2O in nmol L^{-1}), freshwater discharge ($\text{m}^3 \text{s}^{-1}$) and water temperature ($^{\circ}\text{C}$) in the Congo River mainstem at Kisangani (2013-2017). Dotted lines indicate the linear regression. Freshwater discharge value in brackets (2017) was excluded from the regression analysis.

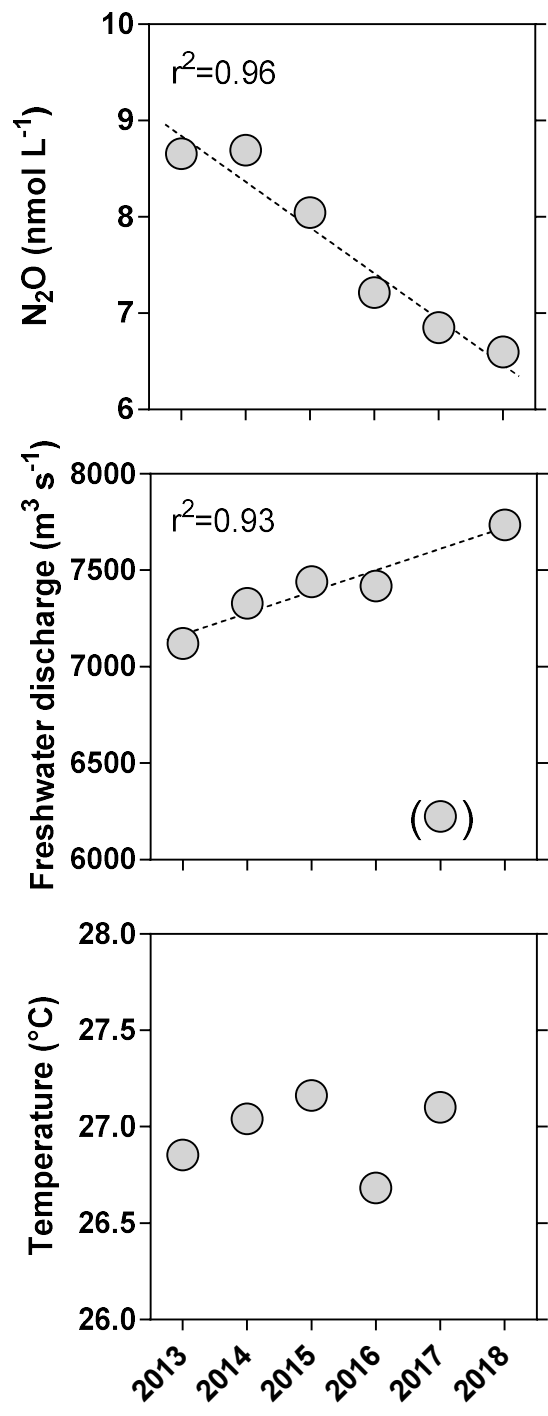


Figure S14: Partial pressure of CO₂ (pCO₂ in ppm) as a function of freshwater discharge (m³ s⁻¹) in the Congo River mainstem at Kisangani (2017-2018).

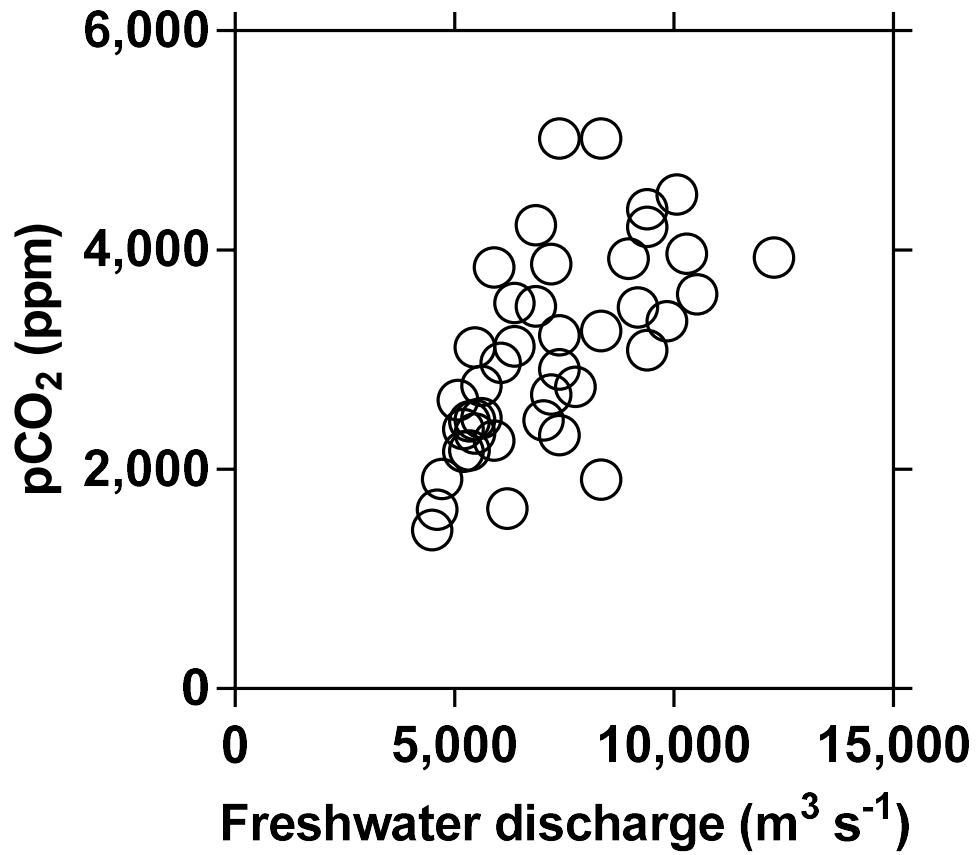


Figure S15: Variation of median gas transfer velocity (k_{600} in cm h^{-1}) and stream surface area (km^2) as a function of Strahler stream order in the Congo River network.

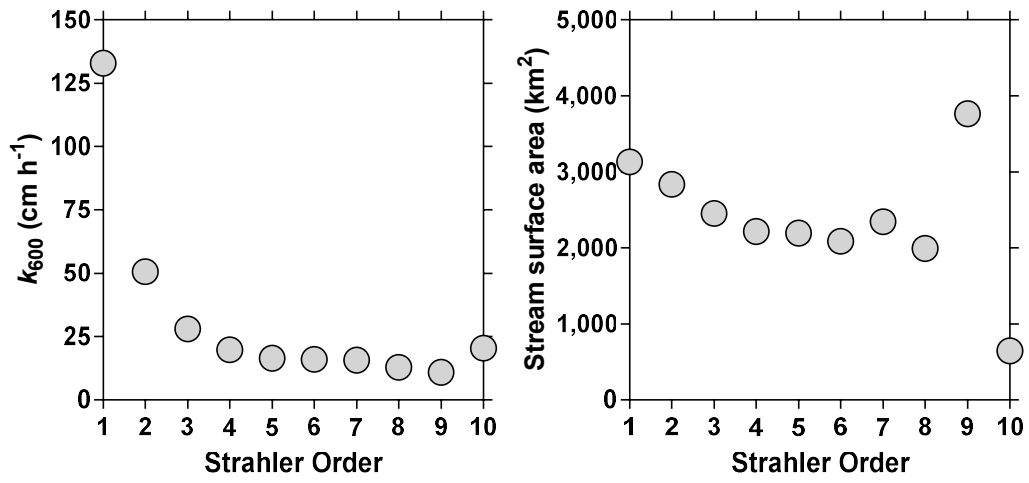


Figure S16: Median partial pressure of CO₂ (pCO₂ in ppm), CH₄ concentration (nmol L⁻¹) and N₂O (nmol L⁻¹) as a function of Strahler stream order in the Congo River network for rivers and streams draining and not draining the Cuvette Centrale Congolaise. Data for order 1 were extrapolated either by considering the same value as for order 2 or with a linear regression (dotted lines).

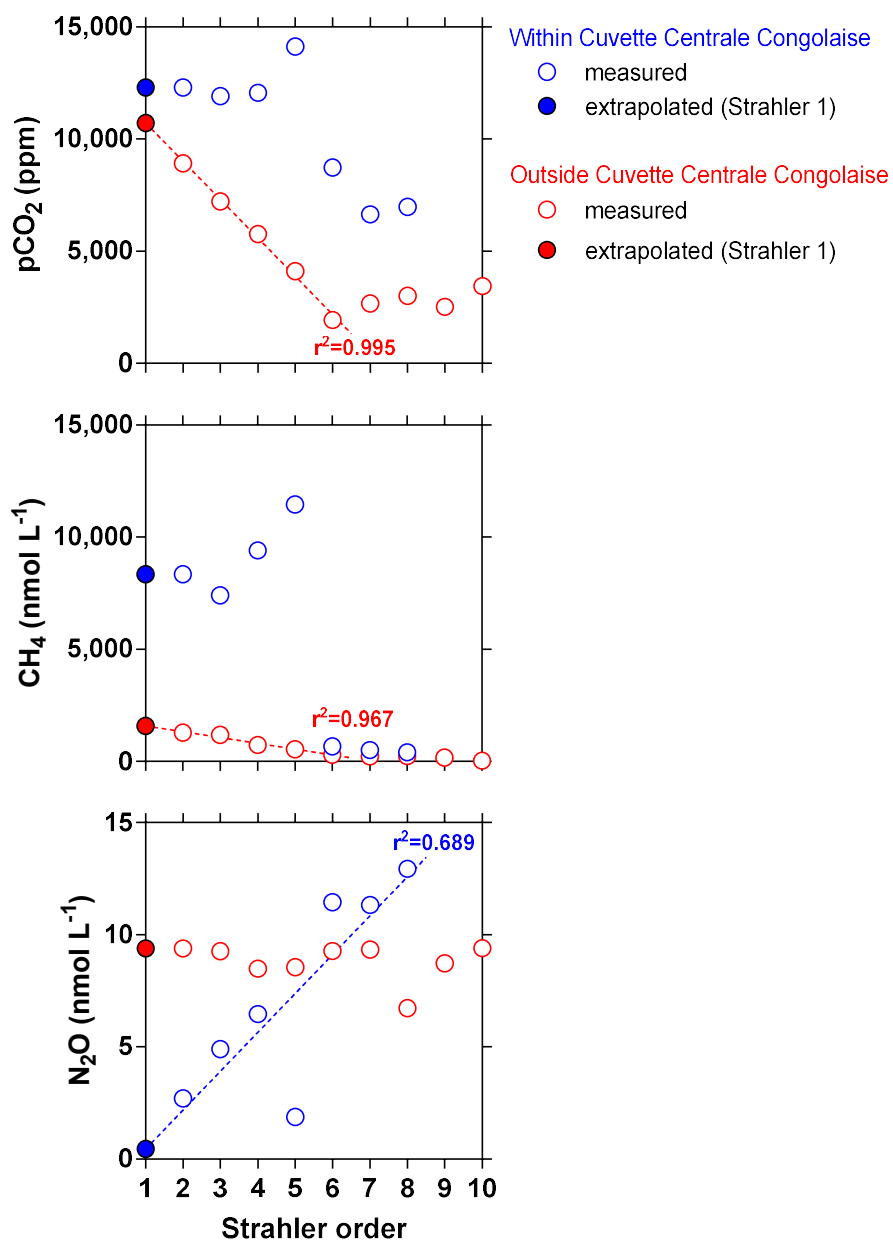


Figure S17: Air-water fluxes of CO₂ (FCO_2 in $\text{mmol m}^{-2} \text{d}^{-1}$), of CH₄ (FCH_4 in $\mu\text{mol m}^{-2} \text{d}^{-1}$), of N₂O (FN_2O in $\mu\text{mol m}^{-2} \text{d}^{-1}$) in the Lualaba at Kisangani as a function of freshwater discharge ($\text{m}^3 \text{s}^{-1}$). Fluxes were computed as explained in the material and methods section from flow velocity derived from freshwater discharge with the hydraulic equation given by Raymond et al. (2012). Dotted lines indicate linear regression.

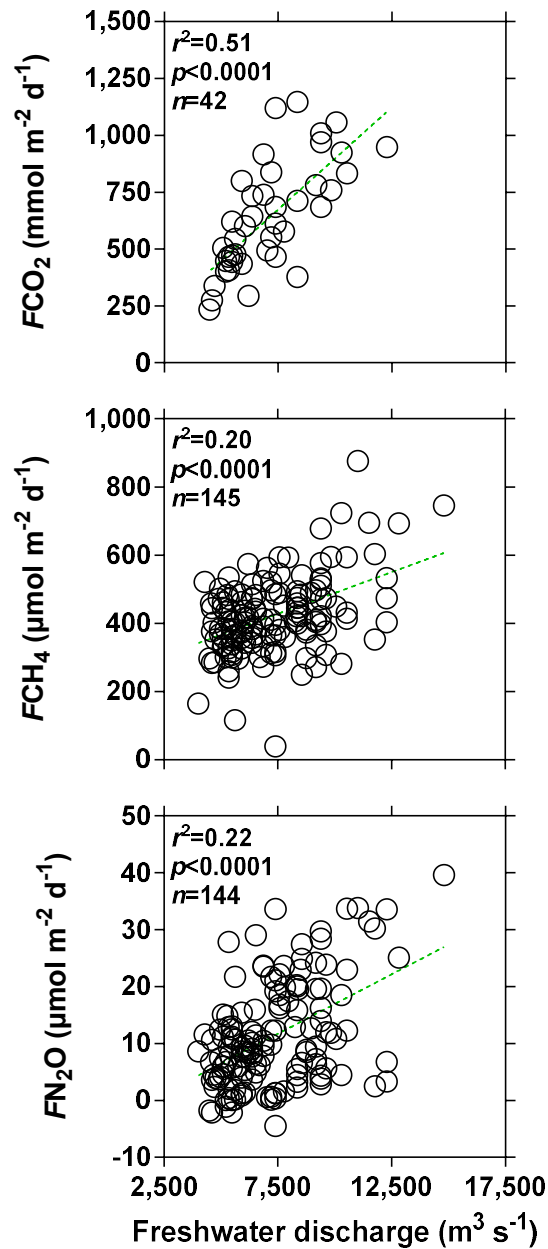
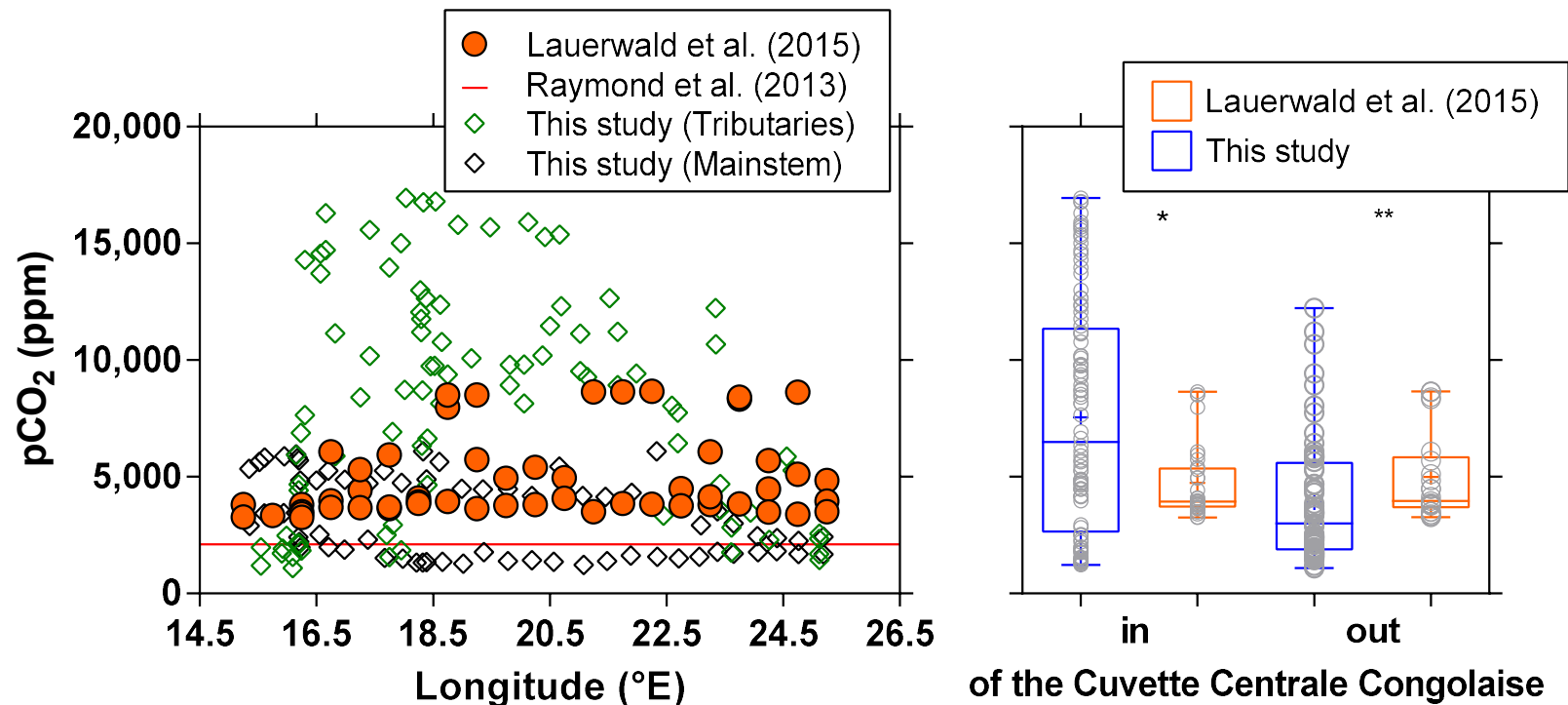


Figure S18: Field data of the partial pressure of CO₂ (pCO₂ in ppm) in tributaries (green symbols) and mainstem (black symbols) of the Congo River (03/12/2013-19/12/2013, 10/06/14-30/06/14), and the output of the model of Lauerwald et al. (2015) at proximity of the sampled sites as function of longitude (°E), as well as the average basin-wide pCO₂ value for the Congo River used by Raymond et al. (2013). Box plot of pCO₂ in surface waters of rivers and streams of the Congo River network draining and not draining the Cuvette Centrale Congolaise from field measurements (03/12/2013-19/12/2013; 10/06/14-30/06/14) and the output of the model of Lauerwald et al. (2015) (orange dots). Field data (both mainstem and tributaries, blue) were significantly higher than model output (red) (Mann-Whitney, p=0.0119) for systems draining the Cuvette Centrale Congolaise but significantly lower than model output (Mann-Whitney, p=0.0044) for systems outside the Cuvette Centrale. The box represents the first and third quartile, horizontal line corresponds to the median, the cross to the average, error bars correspond to the maximum and minimum, symbols show all data points. Although the model of Lauerwald et al. (2015) provides pCO₂ values that are more consistent with observations than the basin-wide average value used by Raymond et al. (2013), the model fails to represent the increase of pCO₂ in rivers draining the Cuvette Centrale Congolaise. This statistical model predicts the fluvial pCO₂ from the net primary production on *terra firme* (as well as slope, air temperature and population density), so fails to account for the influence from wetland carbon inputs.



S1. Spatial analysis

We applied geospatial and statistical methods to compute river width, length, Strahler stream order, surface area, slope, flow velocity, and discharge throughout the Congo River network. All geographic information system (GIS) work was done in ArcMap 10.5 and further geospatial and statistical data analysis was done in R version 3.5.1. The R codes used in this statistical analysis are freely available in the following repository: <https://github.com/geoallen/CongoRiverAnalysis>. We used the following geospatial datasets as input to this analysis:

- 1) The 30-m Global River Widths from Landsat Dataset (GRWL) Version 1.0 summary statistics polyline shapefile (Allen and Pavelsky, 2018);
- 2) The 15-arcsecond HydroSHEDS hydrography flowline dataset (Lehner et al., 2008);
- 3) The HydroSHEDS hydraulically-conditioned digital elevation model (DEM; Lehner et al., 2008);
- 4) The HydroSHEDS river network connectivity tables from Allen et al. (2018) generated using Reproducible Routing Rituals (<https://github.com/c-h-david/rrr>).
- 5) The Global Land Cover (GLC) 2009 dataset from the European Space Agency (http://due.esrin.esa.int/page_globcover.php);
- 6) The Global Lakes and Wetland Database (GLWD) Level-1 product (Lehner and Döll, 2004);
- 7) The HydroBASINS watershed delineation dataset (Lehner and Grill, 2013);
- 8) The river hydrography dataset published in (Andreadis et al., 2013).

S1.1. Data preprocessing

We clipped all geospatial data layers to the Congo Basin using the HydroBASINS dataset. To delineate the Cuvette Centrale Congolaise (CCC) region, we converted the GLC dataset from raster to polygon vector, and then selected polygon regions in the central Congo basin classified as “Closed to Open Broadleaved Forest Regularly Flooded (Fresh-brackish Water)”. We computed all hydrologic parameters (width, length, slope, order, flow velocity, discharge) over the length-scale of a HydroSHEDS river segment, defined as the flowline vector connecting two river network nodes. Using the same procedure as presented in Allen et al. (2018a), we calculated river segment length from the HydroSHEDS flowline dataset and calculated river slope by extracting the elevation of each flowline segment endpoint from the HydroSHEDS DEM and dividing the upstream difference in elevation by the segment length.

S1.2. Spatial join

We fused river width observations from GRWL to HydroSHEDS flowlines using the following spatial join operation: all HydroSHEDS flowlines with a calculated Strahler stream order greater than 4 within 1-km radius of a GRWL centerline was assigned the nearest segment-averaged GRWL river width (Figure S19). Limiting the assignment of GRWL data to segments with orders greater than 4 prevented river widths being assigned to small HydroSHEDS tributaries that do not correspond with the wide rivers in GRWL. We calculated Strahler stream order (Strahler, 1957) in R using HydroSHEDS connectivity tables (Figure S20). Because HydroSHEDS has been shown to be missing at least one stream order (Benstead and Leigh, 2012), we increased the calculated stream order by one after Raymond et al. (2013), such that 1st order segments became 2nd order, 2nd order segments became 3rd order, etc. Rivers within the CCC region were identified by applying a one-to-one intersection spatial join operation between the GLC-derived CCC region and the HydroSHEDS flowline segments. Similarly, we flagged lakes and reservoirs in the flowline dataset by applying a one-to-one intersection of HydroSHEDS flowlines with the GLWD data product. These flagged lakes and reservoirs were removed from the statistical analysis that is described below.

S2. Statistical analysis

The following text and figures describe the procedure for calculating the width, length, surface area, slope, flow velocity, and discharge of rivers and streams by order within the Congo river basin.

S2.1. River surface area

To estimate the surface area of low-order rivers and streams where the input datasets do not contain observations, we used a width-order and length-order statistical scaling approach similar to that used by Raymond et al. (2013). Long-standing fractal river network theory and observational data show that, within a basin, river length, width, and surface area scale exponentially with stream order (Horton, 1945; Strahler, 1957). As stated above, we removed all lakes and reservoirs from the HydroSHEDS flowline dataset so that we were only considering the surface area of rivers and streams (see red flowlines in Figure S19). Then we statistically modeled the median width of rivers with a stream order of 4 or less by fitting a least-squares exponential regression on the median widths of river orders with GRWL-derived observations ($R^2=0.92$, $p=0.002$; Figure S21a).

Similarly, we modeled the total stream length of 1st-order streams by fitting a least-squares exponential regression on the sum length of river orders that we have length estimates ($R^2=0.99$, $p<0.001$; Figure S21b). We computed a sum river and stream surface area (*RSSA*) for each stream order (*i*) by multiplying river width and length,

$$RSSA_i = \sum(Width_i * Length_i). \quad (S1)$$

We used the observed values of width and length where they were available, otherwise we used the modeled values for river segments without observations. We found that 9th-order rivers contain a large proportion of surface area due to their extremely wide and braided morphology in the Congo mainstem (Figure S21c). Summing the surface area of all orders, yielded a total area of 23,670 km² or 0.64% of the Congo basin area (compared to 0.61% as estimated by Raymond et al. (2013) and 0.64% from Allen & Pavelsky (2018)).

To estimate the surface area of rivers wider than 100 m, we calculated the proportion of river length in the GRWL database wider than 100 m for each stream order (Figure S22a). We then multiplied this proportion by the surface area within each stream order (Figure S4b, Table S2-S4) yielding a total surface area of 14,421 km² for rivers and streams narrower than or equal to 100 m and 9,239 km² for rivers wider than 100 m in the Congo basin. Not that, because we limited GRWL data to rivers greater than 4th order, we may not have not observed some third and fourth order rivers that are over 100 m wide. Thus, it is likely that we overestimated the length of rivers narrower than 100 m and underestimated the length of rivers wider than 100 m.

S2.2. Slope, flow velocity and discharge

We used slope-order scaling to estimate the median slope of 1st-order streams in the Congo basin, where HydroSHEDS does not contain information. Consistent with Flint's Law (Flint, 1974), we found that the observed median slope is related to order based on a power-law function (Figure 22a). We apply a least-square power-law regression to extend this relationship to 1st order streams ($R^2=0.95$, $p<0.001$; Figure S23a). To calculate flow velocity (u), we used Manning's formula,

$$u = n^{-1} R^{2/3} S^{1/3}, \quad (S2)$$

where n is Manning's roughness coefficient, assumed to have a mean value of 0.035, R is the hydraulic radius, and S is river slope. The hydraulic radius is equal to river flow width * depth / (width + 2 * depth) for rectangular cross sections (Manning, 1891). We used estimates of mean annual hydraulic radius in the Congo River basin from the hydrography dataset published in Andreadis et al. (2013). This hydrography dataset was created by developing optimized relationships between gauged-based discharge records and upstream drainage area data from the HydroSHEDS hydrography dataset. Then river width and depth were estimated using downstream hydraulic geometry (Leopold and Maddock, 1953; Moody and Troutman, 2002). Using Equation S2, we calculated flow velocity for orders 2-10. To estimate velocity in 1st-order streams, we applied a least-squares exponential regression between stream order and velocity ($R^2=0.88$, $p<0.001$; Figure S23b). Although this produces

an unintuitive positive relationship between flow velocity and stream order, there is long-standing empirical evidence that shows that mean flow velocity is lower in low-order streams where hydraulic roughness is greatest (Leopold and Maddock, 1953). We developed an exponential regression between stream order and the mean annual discharge estimates from Andreadis et al. (2013), and use this statistical relationship to estimate the median discharge of 1st-order streams in the Congo River basin ($R^2 > 0.99$, $p < 0.001$; Figure S23c). Tabulated hydrologic data for the Congo River basin are shown in Table S2.

S3. Spatial estimates inside and outside the CCC region

To estimate river and stream hydrologic parameters inside the Cuvette Centrale Congolaise (CCC) region, we employed the same methods as described above except for two differences: First, we only conducted the statistical analysis on flowlines that were within the CCC area (shown as blue lines in Figure S19). Second, when estimating median river width for stream orders 1-4, we did not include stream order 9 in the least-squares regression because doing so produced unrealistically wide low-order stream widths. This outcome occurred because the 9th-order median river width within the CCC is extremely wide: wider than 5 km, a value more than 8 times the magnitude of 8th-order median river width in the CCC. The 9th-order median width is an outlier because of the relatively small geographic area of the CCC and the unrepresentative wide 9th-order main stem of the Congo River that dominates the river and stream surface area in the CCC region. Estimates for length, slope, flow velocity, and discharge were all based on the exact same methods as those described above. Similarly, for hydrologic parameters outside the CCC region, we used the same methods as described in the sections above except that we removed all rivers and streams within the CCC region in the statistical analysis portion of the analysis. Tabulated statistics for river and stream characteristics are available for inside and outside the CCC region in Table S3 and Table S4, respectively.

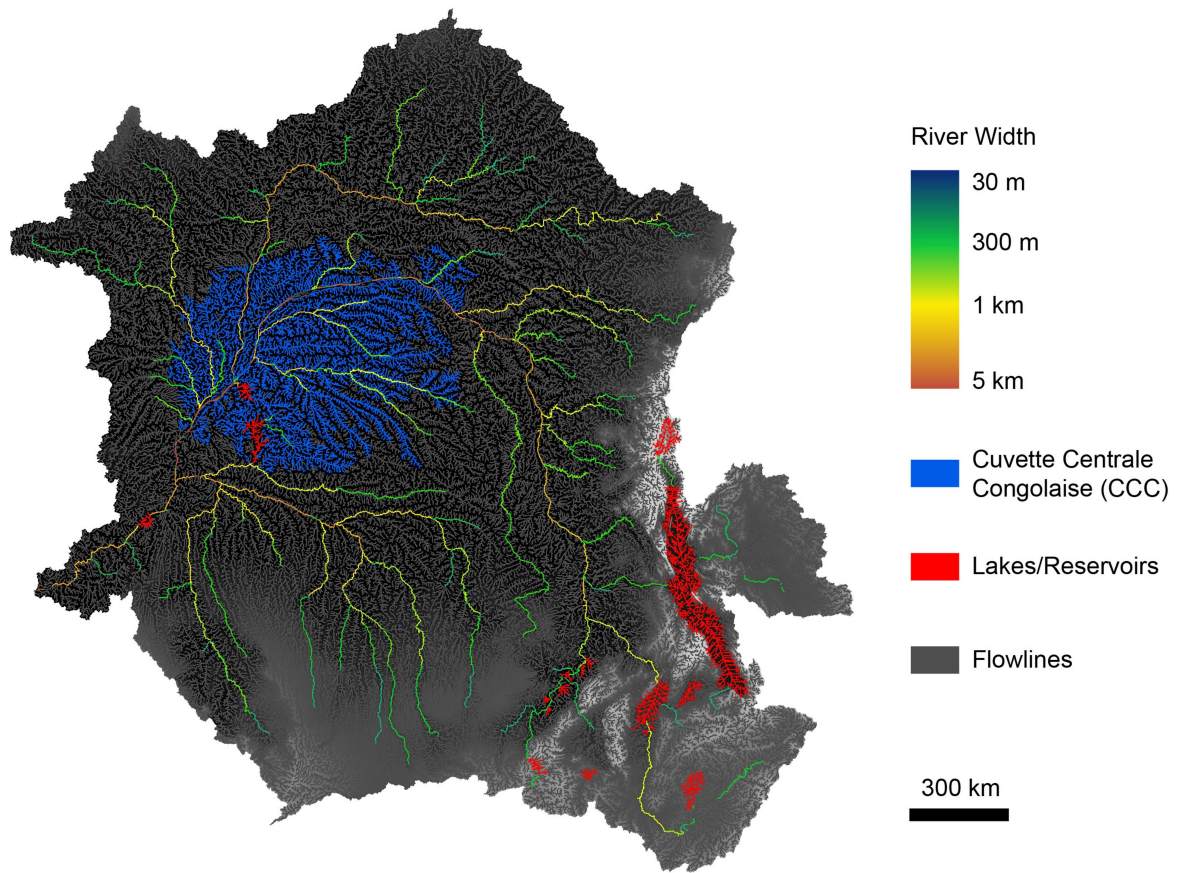


Figure S19: HydroSHEDS flowlines with river widths from GRWL, CCC region from the GLC dataset, and Lakes/Reservoirs from the GLWD. Land surface elevation is shown in the background.

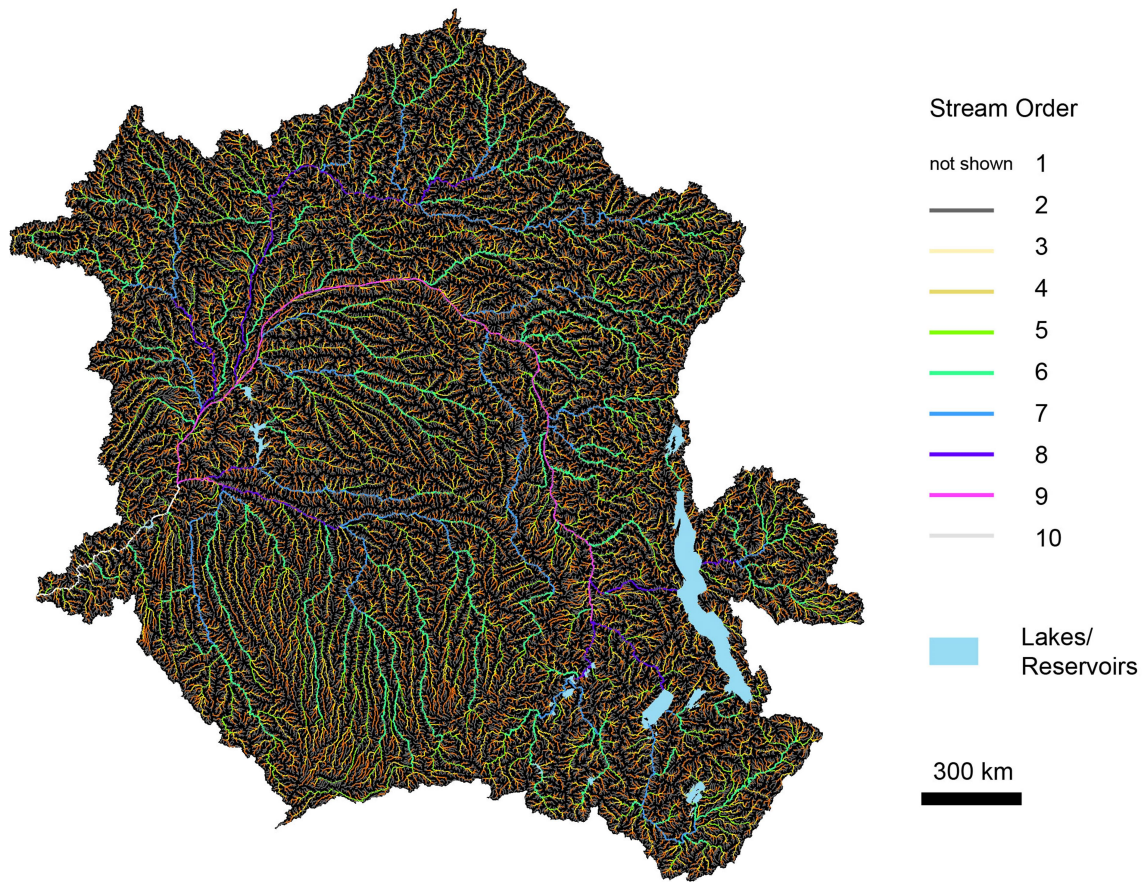


Figure S20: Congo River network colored by Horton-Strahler stream order.

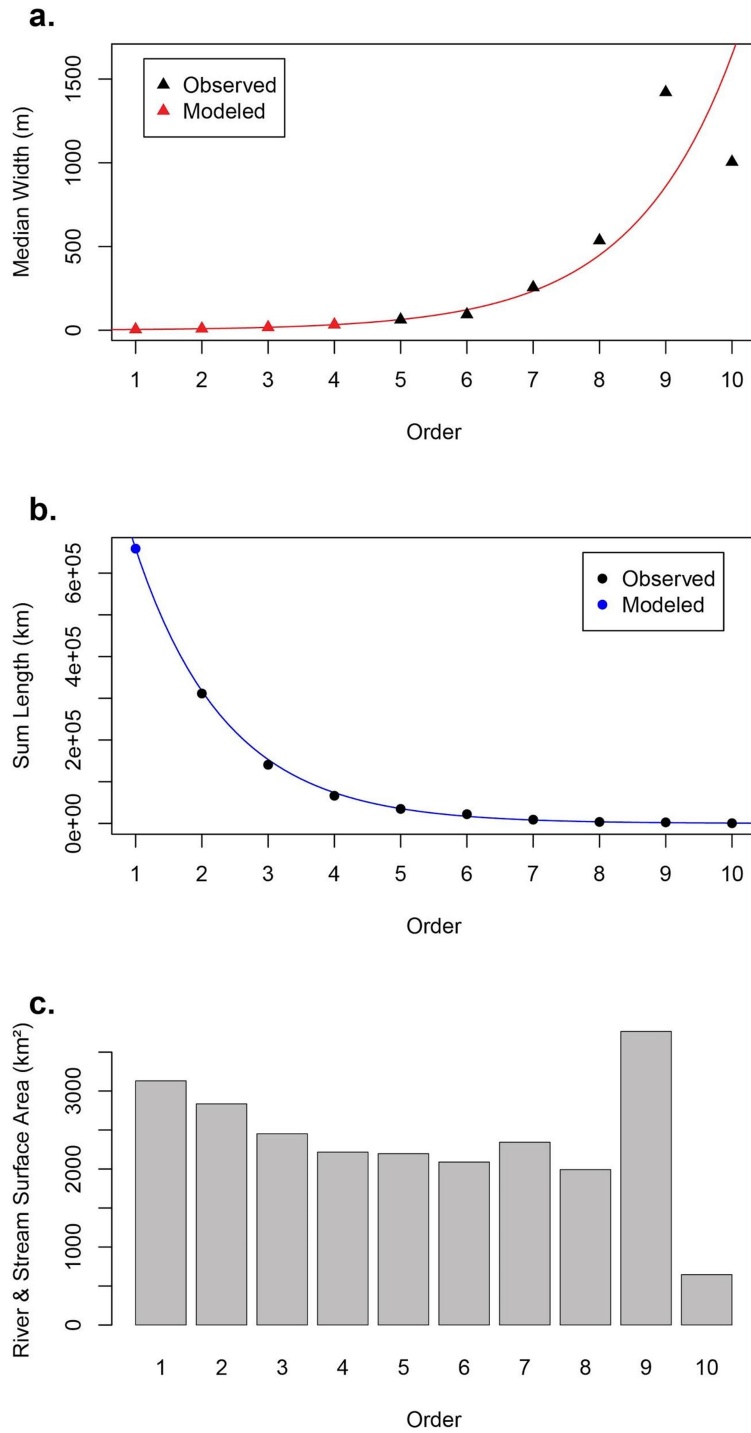


Figure S21: Statistical approach used to estimate: (a) river and stream width; (b) river and stream length; and (c) river and stream surface area by stream order. The large surface area exhibited by 9th-order rivers corresponds to the very wide and braided section of the Congo mainstem

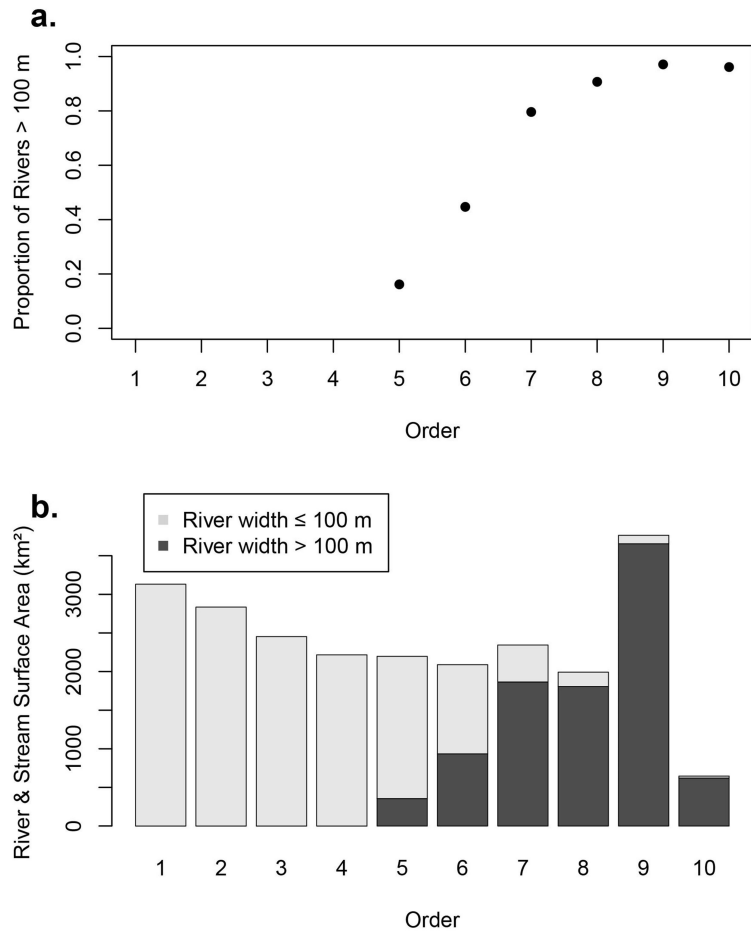


Figure S22: Binning river surface area by width in the Congo Basin. (a) Proportion of rivers wider than 100 m by stream order and (b) Surface area of narrow and wide rivers by river stream order.

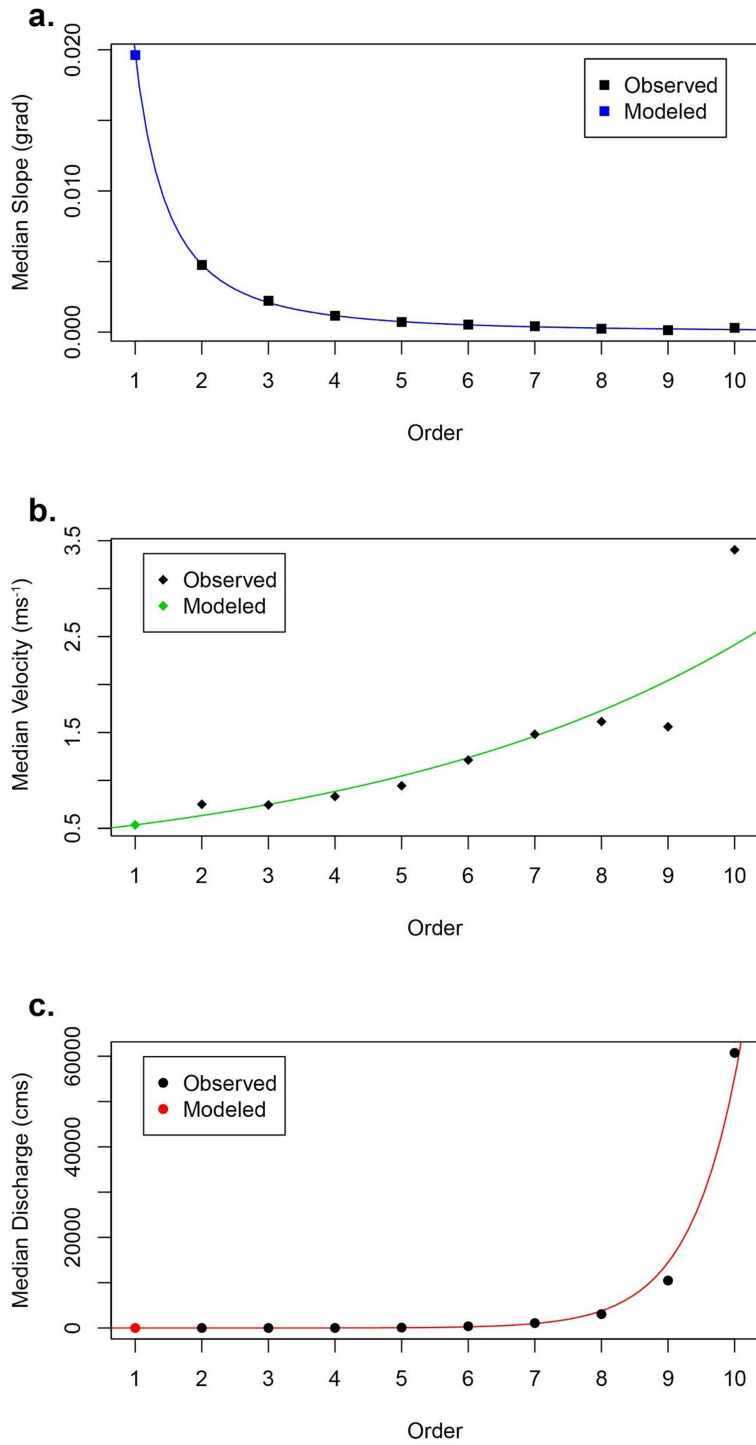


Figure S23: Statistical approach used to calculate 1st-order median stream (a) slope, (b) velocity, and (c) discharge.

Table S1: Annual average freshwater discharge of the main tributaries ($>300 \text{ m}^3 \text{ s}^{-1}$) of the Congo (Rodier 1983).

River name	Left/right bank	Freshwater discharge ($\text{m}^3 \text{ s}^{-1}$)
Lobaye	Left bank	355
Itimbiri	Right bank	356
Lefini	Right bank	388
Alima	Right bank	575
Lindi	Right bank	1200
Lomami	Left bank	1214
Sangha	Right bank	1715
Aruwimi	Left bank	2200
Ruki	Left bank	4200
Oubangui	Right bank	4340
Lualaba	-	6400
Kwa	Left bank	11320

Table S2: Tabulated river and stream statistics for the entire Congo River basin.

Order	Median Width (m)	Sum Length (km)	Sum Area (km ²)	Sum Area of Rivers wider 100 m (km ²)	Median Slope	Median Velocity (mps)	Median Discharge (cms)
1	4.8	658608	3132	0	0.01963	0.536	0.0196
2	9.1	311398	2835	0	0.004747	0.751	0.95
3	17.4	140702	2453	0	0.00222	0.745	4.04
4	33.4	66437	2217	0	0.001155	0.833	19.58
5	63	34877	2197	356	0.000715	0.944	84.94
6	94	22228	2089	934	0.000534	1.212	376.99
7	256	9156	2344	1866	0.000416	1.481	1088.045
8	536	3717	1992	1807	0.000236	1.613	3066.265
9	1421	2649	3765	3656	0.000138	1.559	10474.91
10	1005	643	646	621	0.000297	3.405	60741.16

Table S3: Tabulated river and stream statistics for the Cuvette Centrale Congolaise within the Congo River basin.

Order	Median Width (m)	Sum Length (km)	Sum Area (km ²)	Sum Area of Rivers wider 100 m (km ²)	Median Slope	Median Velocity (mps)	Median Discharge (cms)
1	5.5	63233	350	0	0.004208	0.362	0.0042
2	10.8	31070	335	0	0.001399	0.461	1.22
3	21.1	15359	324	0	0.000768	0.5	5.235
4	41.1	7069	291	0	0.000527	0.627	26.72
5	77	3614	278	116	0.000406	0.845	160.84
6	189	2541	480	400	0.000302	1.059	648.45
7	237	688	163	151	0.000233	1.18	1329.67
8	663	552	366	350	0.000272	1.606	3096.65
9	5794	200	1158	1105	9.50E-05	1.647	33726.82

Table S4: Tabulated river and stream statistics for the Congo River basin, excluding the Cuvette Centrale Congolaise.

Order	Median Width (m)	Sum Length (km)	Sum Area (km ²)	Sum Area of Rivers wider 100 m (km ²)	Median Slope	Median Velocity (mps)	Median Discharge (cms)
1	3.9	574398	2235	0	0.022787	0.568	0.0228
2	7.6	280328	2143	0	0.005158	0.787	0.92
3	15	125343	1883	0	0.00244	0.786	3.9
4	29.5	59368	1752	0	0.00127	0.868	18.71
5	54	31263	1688	199	0.000774	0.962	78.15
6	90	19687	1772	686	0.000571	1.24	334.055
7	256	8468	2168	1702	0.00044	1.52	1076.23
8	536	3164	1696	1523	0.000234	1.613	2956.56
9	1421	2450	3481	3384	0.000144	1.553	10466.86
10	1005	643	646	621	0.000297	3.405	60741.16

References

- Allen, G. H. and Pavelsky, T. M.: Global extent of rivers and streams, *Science*, doi:10.1126/science.aat0636, 2018.
- Allen, G. H., David, C. H., Andreadis, K. M., Hossain, F. and Famiglietti, J. S.: Global Estimates of River Flow Wave Travel Times and Implications for Low-Latency Satellite Data, *Geophysical Research Letters*, 45(15), 7551–7560, doi:10.1029/2018GL077914, 2018a.
- Allen, G. H., David, C. H., Andreadis, K. M., Hossain, F. and Famiglietti, J. S.: Supporting Datasets Produced In Allen Et Al. (2018) Global Estimates Of River Flow Wave Travel Times And Implications For Low-Latency Satellite Data", , doi:10.5281/zenodo.1015799, 2018b.
- Andreadis, K. M., Schumann, G. J. P. and Pavelsky, T. M.: A simple global river bankfull width and depth database, *Water Resources Research*, doi:10.1002/wrcr.20440, 2013.
- Benstead, J. P. and Leigh, D. S.: An expanded role for river networks, *Nature Geosci*, 5(10), 678–679, doi:10.1038/ngeo1593, 2012.
- Flint, J. J.: Stream gradient as a function of order, magnitude, and discharge, *Water Resour. Res.*, 10(5), 969–973, doi:10.1029/WR010i005p00969, 1974.
- Horton, R. E.: Erosional Development of streams and their drainage basins; hydrophysical approach to quantitative morphology, *Geological Society of America Bulletin*, 56(3), 275–370, doi:10.1130/0016-7606(1945)56[275:edosat]2.0.co;2, 1945.
- Lauerwald, R., Laruelle, G. G., Hartmann, J., Ciais, P., and Regnier, P. A. G.: Spatial patterns in CO₂ evasion from the global river network, *Global Biogeochem. Cycles*, 29, 534–554, doi:10.1002/2014GB004941, 2015.
- Lehner, B. and Döll, P.: Development and validation of a global database of lakes, reservoirs and wetlands, *Journal of Hydrology*, 296(1–4), 1–22, doi:10.1016/j.jhydrol.2004.03.028, 2004.
- Lehner, B. and Grill, G.: Global river hydrography and network routing: baseline data and new approaches to study the world's large river systems, *Hydrological Processes*, 27(15), 2171–2186, doi:10.1002/hyp.9740, 2013.
- Lehner, B., Verdin, K. and Jarvis, A.: New Global Hydrography Derived From Spaceborne Elevation Data, *Eos Trans. AGU*, 89(10), doi:10.1029/2008eo100001, 2008.
- Leopold, L. B. and Maddock, T., Jr.: The hydraulic geometry of stream channels and physiographic implications, *USGS Prof. Paper*, 57, 1953.
- Manning, R.: On the flow of water in open channels and pipes, *Transactions of the Institution of Civil Engineers of Ireland*, 20, 161–207, 1891.
- Moody, J. A. and Troutman, B. M.: Characterization of the spatial variability of channel morphology, *Earth Surface Processes and Landforms*, 27(12), 1251–1266, doi:10.1002/esp.403, 2002.

Raymond, P. A., Zappa, C. J., Butman, D., Bott, T. L., Potter, C., Mulholland, P., Laursen, A. E., McDowell, W. H., and Newbold, D.: Scaling the gas transfer velocity and hydraulic geometry in streams and small rivers. *Limnol. Oceanogr. Fluids Environ.*, 2, 41-53, doi: 10.1215/21573689-1597669, 2012.

Raymond, P. A., Hartmann, J., Lauerwald, R., Sobek, S., McDonald, C., Hoover, M., Butman, D., Striegl, R., Mayorga, E., Humborg, C., Kortelainen, P., Durr, H., Meybeck, M., Ciais, P. and Guth, P.: Global carbon dioxide emissions from inland waters, *Nature*, 503(7476), 355–359, doi:10.1038/nature12760, 2013.

Rodier, J. A.: Aspects scientifiques et techniques de l'hydrologie des zones humides de l'Afrique centrale, *Hydrology of Humid Tropical Regions with Particular Reference to the hydrological Effects of Agriculture and Forestry Practice (Proceedings of the Hamburg Symposium, August 1983)*, IAHS Publ. no. 140, 1983.

Strahler, A. N.: Quantitative analysis of watershed geomorphology, *Eos, Transactions American Geophysical Union*, 38(6), 913–920, doi:10.1029/TR038i006p00913, 1957.

Still, C. J., and Powell, R. L.: Continental-scale distributions of vegetation stable carbon isotope ratios. West JB, Bowen GJ, Dawson TE, Tu KP, editors. *Isoscapes*. Netherlands: Springer Netherlands. p179-193, 2010.